Finite Element Modeling of micro orthogonal cutting process with Dead Metal Cap

Ali Afsharhanaei [*]**, Lara Rebaioli, Paolo Parenti, Massimiliano Annoni**

Dipartimento di Meccanica, Politecnico di Milano, Milano, Italy

*Corresponding author:

Ali Afsharhanaei, Dipartimento di Meccanica, Politecnico di Milano, via La Masa 1, 20156, Milano, Italy.

Email: ali.afsharhanaei@polimi.it

Abstract

Dead Metal Cap (DMC) plays an important role in the microcutting process because this material piled up on the tool-chip-workpiece interface can alter the cutting geometry. The target of this study is to model and simulate the micro orthogonal cutting process in presence of DMC in order to investigate the effects of this phenomenon on the micromachining process outputs (cutting force, thrust force, chip thickness) and stress distribution, equivalent plastic strain and temperature inside the workpiece shear zones. For this purpose, the Finite Element Method (FEM) with explicit dynamic solution and adiabatic heating effect along with Arbitrary Lagrangian Eulerian (ALE) approach is used. It is shown that the FE models with current state of the art assumptions cannot take into account the DMC by default. For this reason, DMC is artificially introduced on the rounded tool edge in this study for carrying out a proper analysis. Several simulations with different DMC geometries are performed and obtained results show that prediction of cutting force, thrust force and chip thickness are sensitive to the presence of DMC and its geometry. Micro orthogonal cutting experiments are carried out on tubular AISI 1045 workpieces for validating and interpreting simulated results. The error between predicted and experimental data is calculated and it is shown that simulation performances can be improved by considering the DMC into the process model. For example, it is possible to reduce the error to less than 5% in case of thrust force prediction. This study points out how the target material Von Mises stress, equivalent plastic strain and temperature distribution are sensitive to any alteration of the edge geometry due to the DMC. The best DMC configuration in terms of agreement with experiments is also the one introducing a more homogeneous distribution of these quantities along the shear plane.

Keywords: Microcutting, Dead Metal Cap, AISI 1045, Finite Element Analysis, Cutting Forces, Chip Thickness

Nomenclature

A	Initial yield stress at room temperature in Johnson-Cook flow stress model
AB	Arbitrary line beneath the tool rounded edge for determination of velocity
B	Strain hardening coefficient in Johnson-Cook flow stress model
C	Strain rate sensitivity coefficient in Johnson-Cook flow stress model
err_c	Percentage error for cutting force
err_t	Percentage error for thrust force
err_{tc}	Percentage error for chip thickness
E	Elastic modulus
F_c	Cutting force
F_t	Thrust force
k_f	Maximum shear stress
m	Thermal softening exponent in Johnson-Cook flow stress model
n	Strain hardening exponent in Johnson-Cook flow stress model
$N_{1,2,3,4,5}$	Number of nodes defined on line AB for determination of velocity
OS	Shear plane connects stagnation point to pre flow zone
r_e	Tool edge radius
S	Stagnation point
t_c	Chip thickness
t_u	Uncut chip thickness
T_H	Homologous temperature in Johnson-Cook flow stress model
T_{melt}	Melting temperature in Johnson-Cook flow stress model
T_{room}	Room temperature in Johnson-Cook flow stress model
v_1	Velocity in cutting direction (X)

v_2	Velocity in thrust direction (Y)
v_c	Cutting velocity
α	Tool rake angle
α_T	Thermal expansion
β	Tool clearance angle
β_T	Inelastic heat fraction
$\dot{\varepsilon}_0$	Reference strain rate in Johnson-Cook flow stress model
ε	Plastic strain
ζ	DMC rake angle
λ	Thermal conductivity
μ	Coulomb friction coefficient
v	Poisson's ratio
ρ	Density
σ	Equivalent flow stress
σ_y	Yield stress
ψ	DMC clearance angle

1. Introduction

The demand for production of very small parts and features is increasing and micromachining is one of the most frequently used process for manufacturing 3D miniaturized products because of its applicability to a wide range of materials, its flexibility and moderate cost[1]. For example, micromachining allows to create products for the biomedical and the aerospace sectors, micro molds for the microinjection process and small-size high-tech parts for the electronics sector.

Besides the broad application of this manufacturing process, its basic phenomena still need to be fully understood, thus making the machining modeling in the micro scale more complex than in the macro scale. The complete determination of these phenomena would provide two important advantages: 1) a better modeling of tool–workpiece interaction, which leads to the prediction of the machine tool behavior and, as a result, a better design and manufacturing of machine components; 2) a better prediction of the cutting process final output, which helps the end users to design the machining operations for the target product.

Going into further details, the modeling of machining operations in the macro scale has to face the complexity associated with the target material flow stress and contact behavior. In addition, the size effect adds more complexity to the process modeling in the micro scale, representing a challenge for accurate predictions. In fact, when the uncut chip thickness is comparable in size to the critical tool geometrical features, as the cutting edge radius, the effective rake angle[2,3] gains an important role in the chip formation, the ploughing action becomes more relevant than the shearing action and the specific energy consumption for the material removal changes non-linearly with the uncut chip thickness reduction[4]. In addition, the material microstructure increases its effectiveness on cutting forces, since the critical tool geometrical features tend to have the same magnitude order of the material grains[4]. Micromachining is also affected by the Minimum Uncut Chip Thickness (MUCT) effect[5], meaning that the chip does not form when the uncut chip thickness is below a critical value and ploughing takes place instead of shearing.
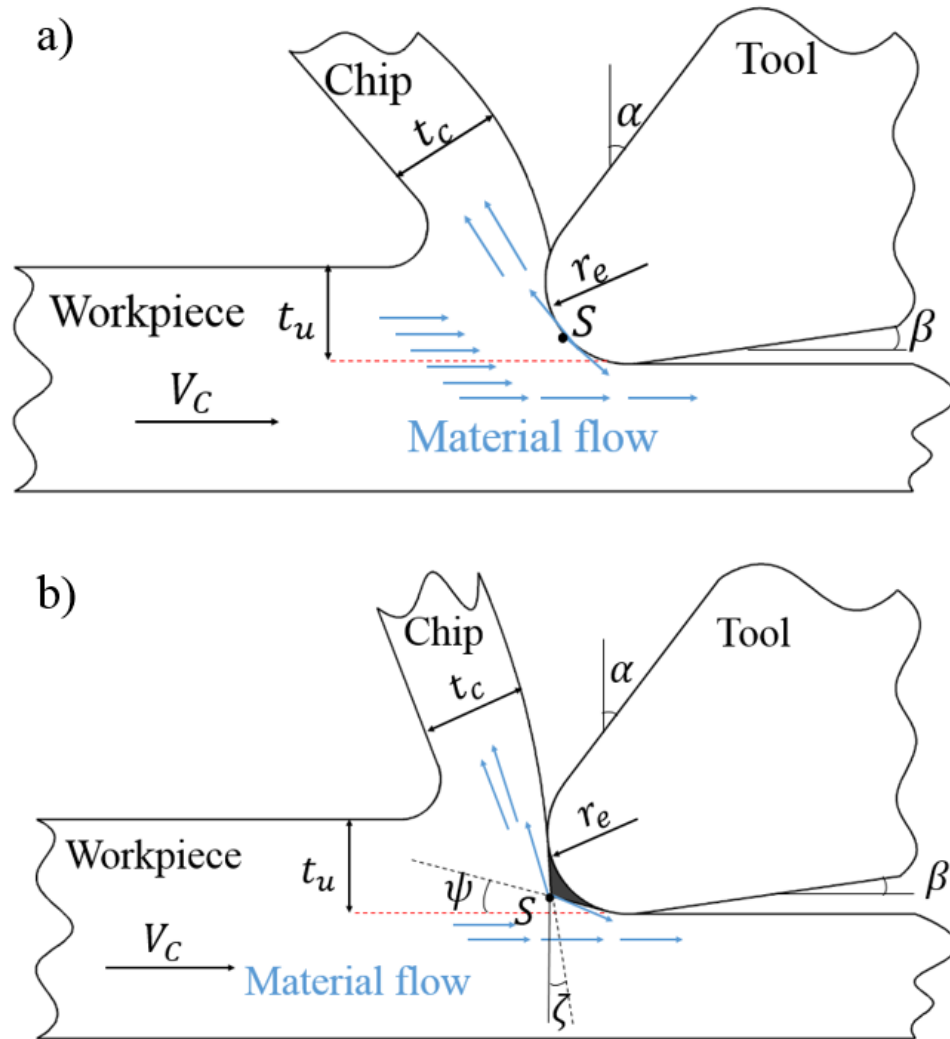
Figure 1. Material flow in microcutting: a) stagnation point (S) on tool edge radius; b) stagnation point (S) on Dead Metal Cap (DMC)

Figure 1 indicates two possible models of the material flow in front of the tool cutting edge. In Figure 1a, the material flow separates at the tool cutting edge in front of the stagnation point S. Figure 1b introduces the Dead Metal Cap (DMC) that is an amount of piled up material stuck around the tool cutting edge. DMC is similar to Built-Up Edge (BUE) but is stable (in fact, in some research works it is referred as stable BUE[6,7]) and its existence does not depend on the cutting velocity[8]. With the presence of DMC (Figure 1b), flow zone and stagnation point move away from the tool cutting edge, this way modifying the whole microcutting geometry and leading to unexpected process behaviors in terms of chip formation and force magnitude.

Providing experimental evidence of the DMC presence is a challenging task due to the phenomenon scale but there are some research works proving the DMC existence[6,9,10]. For instance, Abdelmoneim and Scrutton[6] performed quick-stop experiments on free-cutting brass (CuZn36Pb3) and noticed a stable built-up edge. Warnecke[9] was one of the first researchers who observed the cutting process by means of a high speed camera for different cutting velocity ranges and proved that DMC exists for AISI 1045 steel. The study of Kountanya and Endres[10] was based on high magnification visualization of the cutting process and confirmed the presence of piled up material in front of tool edge for cartridge brass (CuZn30) but not for commercially pure zinc.

Throughout literature, DMC has been investigated by means of experimental works and analytical or numerical models. Jacobson and Wallen[11–13] performed an experimental investigation of the Dead Metal Cap effect on the intermittent cutting of plain carbon steel (AISI 1045) and austenitic stainless steel (AISI 316) and proposed a classification of dead zones in the cutting process. Furthermore, Abdelmoneim and Scrutton[6] obtained upper-bound solutions to a theoretical analysis of the metal cutting process with stable built up edge created in machining of free-cutting brass (CuZn36Pb3) and found an agreement between theoretical analysis and experimental data.

Analytical models and, in particular, slip-line field models, are widely used since they are easier to implement and require a lower computational time than numerical models[14]. For example, Waldorf et al.[7] proposed a slip-line field model for studying the case of rounded tool edge in presence of DMC and were able to predict both ploughing and shearing forces in orthogonal cutting of 6061-T6 aluminium. The same authors[15] performed a comparison between two slip-line field solutions (with and without DMC) for machining 6061-T6 aluminium and found that the model considering DMC could provide a better estimation of experimental results. In other papers, Karpat and Özel[16] used a slip-line field model including DMC to study the mechanics and friction in orthogonal cutting of AISI 4340 steel with rounded tools while Jun et al[17] developed a model for cutting force prediction in micro end milling that is based on a slip-line field model considering DMC. Nevertheless, it should be pointed out that slip-line field models are based on the strong assumption that the target material is perfectly rigid plastic[18] and they provide unique solution for each machining problem[14] so these facts limit their prediction performance.

Finite Element Analysis (FEA) is another technique that plays a significant role in DMC modeling, since it can include a wide variety of material flow stress models and it can directly provide information on industrially relevant outcomes (such as chip shape, burrs and surface finish)[14]. For instance, some studies focused on predicting DMC formation beneath the tool cutting edge for P20[19] and AISI 1045[20] steels by representing the material plastic flow through the Johnson-Cook flow stress model, even if this assumption is against the fact that DMC is the result of a ductile shear failure since the Johnson-Cook flow stress model cannot take into account the material failure. Childs[21] performed FEA of AISI 5130 steel machining including a ductile shear failure model in order to predict the formation and geometry of built-up edge in macro cutting and DMC in microcutting, but he concluded that his model could not follow the evolution of these phenomena. In fact, a limitation of FE models is that they cannot take into account the DMC basic stationary properties and represent the creation of DMC by means of simple flow stress models without implementation of material failure model.

This paper presents a 2D Finite Element simulation of AISI 1045 orthogonal cutting in the microscale where DMC is artificially introduced to consider its stationary properties and let the target material freely flow on the DMC-chip contact surface. The novelty of developed model is summarized in ability to perform micromachining simulations with presence of DMC. For this study, AISI 1045 steel is selected as target material because of its broad application for basic academic investigations[22] and since microcutting of this material is of interest thanks to its potential to achieve good surface and geometry quality in micro-sized dies and molds[1]. This paper investigates the effects of DMC on the process output parameters (namely cutting and thrust forces, chip thickness and stress, strain and temperature distributions within the workpiece deformation zones) and validates the FEM results by comparing them with data coming from microcutting experiments.

2. Finite Element Modeling of micro orthogonal cutting

2.1. Modeling setup definition

Two-dimensional micro orthogonal cutting on AISI 1045 steel is modeled. The DMC geometry is artificially introduced on the tool edge surface. Based on the experimental

observations of Warnecke[9] and Kountanya[10], the DMC is modelled with a sharp corner edge and smooth faces (Figure 1b). According to the theory of Jun et al.[17], the two faces of DMC are tangent to the tool edge radius to facilitate the material flow over rake and clearance faces. To make DMC fully constrained in space, it is necessary to introduce two angles, namely, rake ζ and clearance ψ angles of DMC (Figure 1b).

In this study, two values for both ζ and ψ angles are selected in order to investigate the effects of DMC geometry and to perform a sensitivity analysis on the FEM output variables with respect to DMC angles. Figure 2 shows the different DMC geometries on the tool edge that result from varying angle ζ and ψ. A rounded tool edge is also used in finite element simulations to allow a result comparison (Section 4).
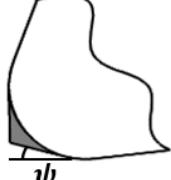
Case 1: $\psi = 0°$; $\zeta = 0°$	Case 2: $\psi = 0°$; $\zeta = 15°$	Case 3: $\psi = 15°$; $\zeta = 0°$	Case 4: $\psi = 15°$; $\zeta = 15°$

Figure 2. DMC geometries analyzed in the present study

The workpiece is meshed with quadrilateral continuum elements (CPE4R)[23], which enable the displacement calculation during the analysis and can take into account the adiabatic heating effect. The mesh geometry spreads uniformly throughout the workpiece and the element size is 1 μm × 2 μm. The tool and the DMC, if any, are considered as a unique completely rigid body. The workpiece is designed to be a rectangular with width of 60μm and length of 230 μm which in total includes 7020 elements.

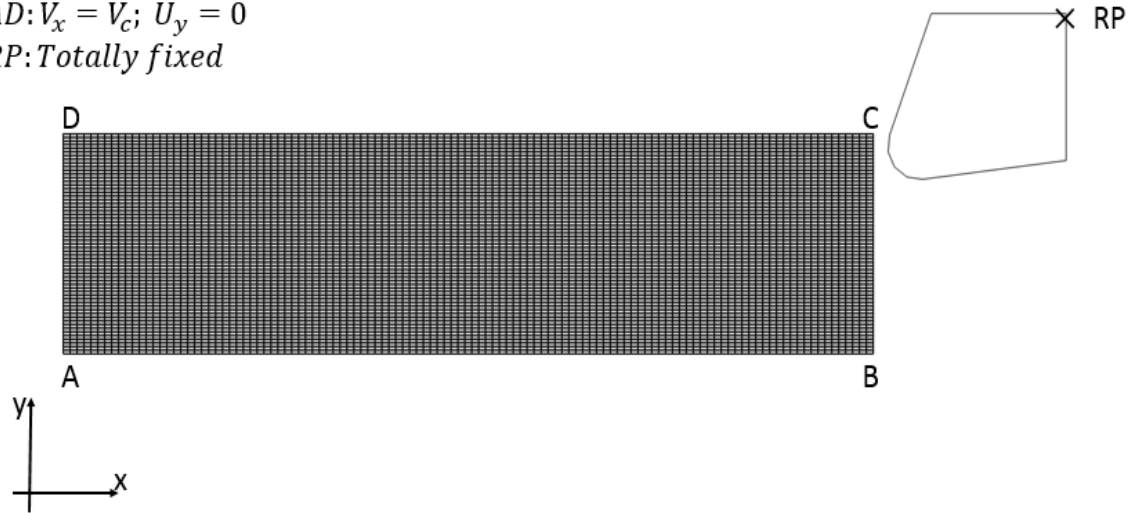$AB: U_y = 0$
$AD: V_x = V_c; U_y = 0$
$RP: Totally\ fixed$

Figure 3. Tool-workpiece assembly with boundary specifications

As depicted in Figure 3, the tool is totally fixed at the reference point (RP), where the simulation outputs are extracted. The workpiece is set as a moving object that is constrained along its bottom side (Line AB in Figure 3) with zero displacement in the Y direction and along its left side (Line AD in Figure 3) with zero displacement in Y direction and velocity in X direction equal to the cutting velocity.

2.2. Solution method

The micro orthogonal cutting operation is simulated by ABAQUS with explicit dynamic solution and adiabatic heating effect along with adaptive Arbitrary Lagrangian Eulerian (ALE) mesh distortion control. Indeed, explicit formulation based on central difference method[23] has been exploited in several studies[24–26] for simulating high speed machining. Finite element analysis of machining considering the adiabatic heating effect has been used and validated in the works of Jin and Altintas[27], and Mabrouki and Rigal [28].

In micromachining simulation, the material undergoes severe deformations and mesh distortion is very likely to occur beneath the tool edge, but ALE technique allows to maintain a high-quality mesh in front of the tool tip. The ALE formulation is a combination of pure Lagrangian technique (where the mesh moves together with the material) and pure Eulerian

technique (where the mesh is fixed in space and the material flows inside the domain). ALE method has been exploited for machining simulation in several research works[19,20,24–26,29,30].

In metal cutting simulations, there are different numerical methods to avoid mesh distortion on workpiece deformation zones, namely ALE, Eulerian, Lagrangian with remeshing-rezoning, and Smoothed-Particle Hydrodynamics (SPH). Advantages and disadvantages of each modeling technique are well described through literature [31–34]. In current work, ALE approach is used because of its capability to simulate machining process with lower computational effort in 2D.

In this field, the ALE approach can be implemented without a chip geometry initialization and with pure Lagrangian boundaries or, alternatively, by initializing the chip geometry and with a combination of Lagrangian and Eulerian boundaries[35]. In this study, the ALE technique is implemented without any chip geometry initialization because the chip shape is unknown when cutting with low uncut chip thickness, i.e. comparable with edge radius of the tool. ALE adaptive mesh domain can be controlled by frequency and number of remeshing sweeps per increment which are set to be 5 and 4 respectively for entire simulations of this study.

2.3. Flow stress model

The Johnson-Cook law[36] is used for modeling the plastic deformation behavior of the selected target material (AISI 1045 steel). This model is formulated as follow:

$$\sigma = [A + B(\varepsilon)^n]\left[1 + C ln\left(\frac{\dot{\varepsilon}}{\dot{\varepsilon}_0}\right)\right]\left[1 - \left(\frac{T - T_{room}}{T_{melt} - T_{room}}\right)^m\right] \tag{1}$$

where σ is the flow stress, A is the initial yield stress at room temperature, B is the strain hardening coefficient, C is the strain rate sensitivity coefficient, m is the thermal softening exponent, n is the strain hardening exponent, ε is the plastic strain, $\dot{\varepsilon}$ is the strain rate, $\dot{\varepsilon}_0$ is the reference strain rate, T is the absolute temperature, T_{room} is the room temperature and T_{melt}

is the melting temperature. The Johnson-Cook parameters[37] and thermo-mechanical properties [26] of the selected target material (AISI 1045) are reported in Table 1.

Table 1. Thermo-mechanical properties of AISI 1045 [26,37]

Parameters	Value
Thermo-mechanical properties[26]	
E: Elastic modulus	200 GPa
ρ: Density	7800 kg/m^3
v: Poisson's ratio	0.3
c : Specific heat	432.6 J/(kg·°C)
α_T: Thermal expansion	11 μm/(m·°C)
λ: Thermal conductivity	47.7 W/(m·°C)
β_T : Inelastic heat fraction	0.9
k_f : Maximum shear stress	319.3 MPa
Johnson-Cook constants[37]	
A: Initial yield stress at room temperature	553.1 MPa
B: Strain hardening coefficient	600.8 MPa
C : Strain rate sensitivity coefficient	0.0134
m : Thermal softening exponent	1
n : Strain hardening exponent	0.234
Johnson-Cook inputs	
$\dot{\varepsilon}_0$: Reference strain rate[37]	1 1/s
T_{melt} : Melting temperature[37]	1460 °C
T_{room} : Room temperature	25 °C

2.4. Contact law

In high speed machining and especially in cutting with low uncut chip thickness, where the tool edge radius plays a significant role on the cutting action, there are interactions within

bodies with complex contact properties due to the high plastic deformation generating high stresses, strains and strain rates. The friction modeling in high speed machining has been the subject of several studies. For instance, Haglund et al.[38] performed the finite element simulations with ALE approach and Eulerian boundaries together with different types of friction models. They concluded that using a shear stress threshold to represent the stick-slip behavior in the contact zone is an inadequate approach for force prediction in models with Eulerian boundaries. However, Arrazola and Özel[35] made a research work discussing different types of friction models in finite element analysis of metal cutting processes. They investigated the applicability of a modified Coulomb friction model with shear stress threshold and two different ALE techniques, concluding that the shear stress limitation can affect the results and becomes effective for the model with Lagrangian boundaries.

In this study, Lagrangian boundaries are selected (Section 2b), hence the modified Coulomb friction model with shear stress threshold (Eq. 3a-3b) is applied to include the stick-slip behavior of the target material in contact with a rigid body, i.e. the tool-DMC assembly. In this study, a constant friction coefficient equal to 0.45 and is used and shear stress limit is adopted by calculating $\sigma_y/\sqrt{3}$, being σ_y the target material yield stress, according to the work by Woon et al. [26], performing the finite element simulation of AISI 1045 micromachining with an ALE approach.

3. Experimental procedure

3.1. Experimental setup

For comparing and validating the FEM results, micro orthogonal cutting tests are performed on an ultra-precision Kern EVO 5 axis machining center with nominal positioning accuracy of $\pm$ 1 µm. Tubular workpieces made of AISI 1045 Steel with a wall thickness of 0.65 mm are turned by SANDVIK standard uncoated carbide inserts (DCGX070202-AL H10). The micro orthogonal cutting setup is shown in Figure 4.

The insert geometry is inspected by means of a 3D optical measuring machine (Alicona Infinite Focus) and the measured edge radius (r_e), rake angle (α) and clearance angle (γ) are 9

µm, 20° and 7° respectively (Figure 5). Measurements of rake and clearance angles are carried out by placing the insert bottom surface in contact with the Alicona Infinite Focus table that is used as reference.
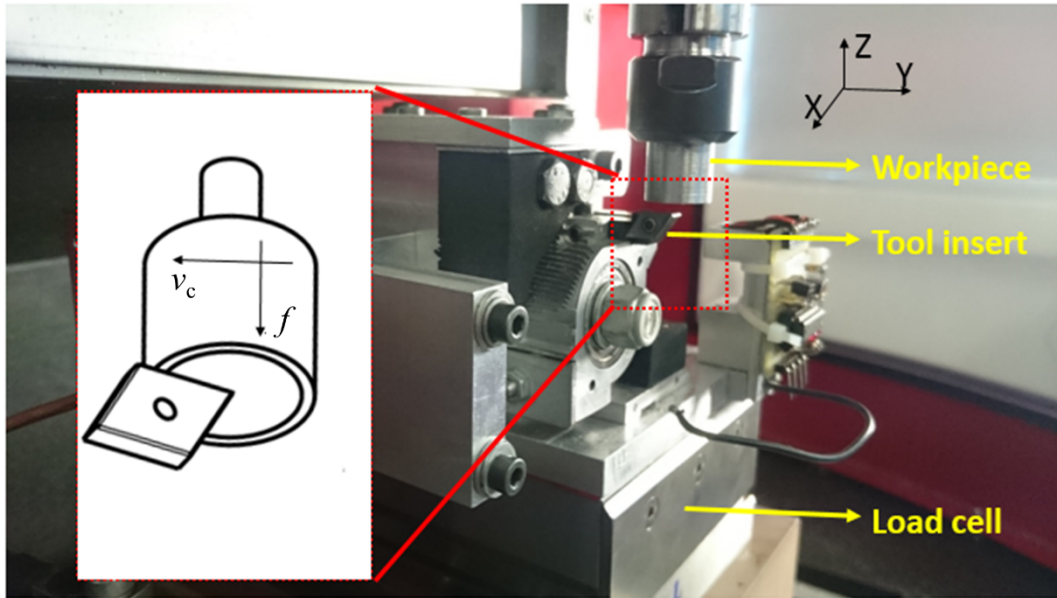

Figure 4. Micro orthogonal cutting setup on a Kern EVO machining center
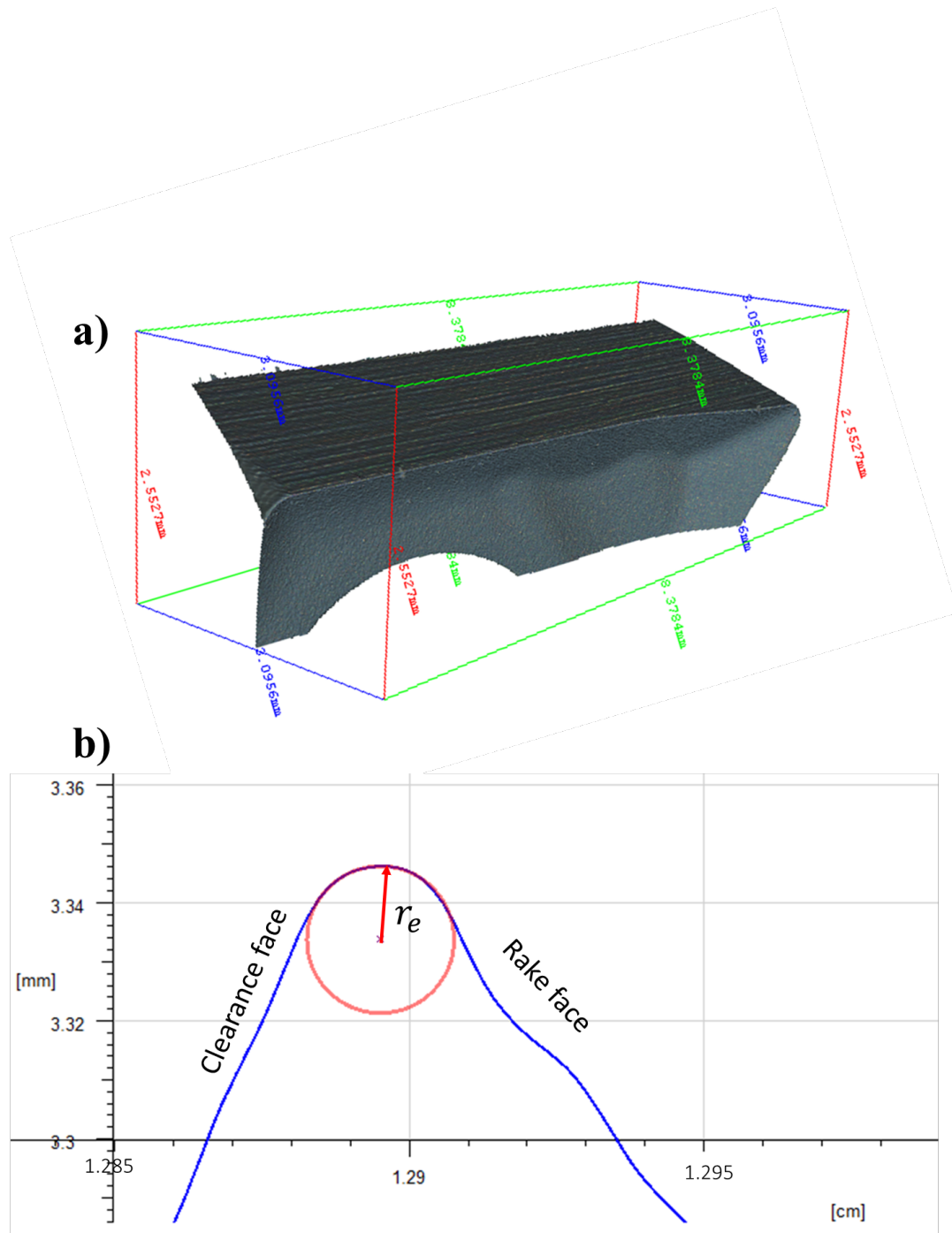
Figure 5. Insert acquisition by Alicona Infinite Focus: a) 3D surface topography; b) edge radius (r_e) measurement

3.2. Experimental design

DMC is placed in front of tool edge radius, hence two uncut chip thickness values (6 and 9 µm) are selected in this study for micro orthogonal cutting experiments in order to study the DMC effects on the process outputs when machining with an uncut chip thickness

comparable to the tool edge radius (r_e = 9 μm). Moreover, two different levels of cutting velocity (100 and 300 m/min) are also considered in this study (in order to investigate if DMC geometry is sensitive to cutting velocity changes) (Table 2). Two replicates are performed for each experimental condition, hence the experimental plan consists of eight runs. The experiments are fully randomized.

Table 2. Experimental conditions

Experimental condition	Cutting velocity v_c (m/min)	Uncut chip thickness t_u (μm)
a	100	6
b	300	6
c	100	9
d	300	9

The experimental study pointed out the willingness of the material to stick on the tool edge radius (Figure 6), this way verifying the DMC existence in microcutting of AISI 1045. SEM analyses of the tool showed that the fresh edge (Figure 6a) is covered by the target material after performing cutting experiments (Figure 6b).
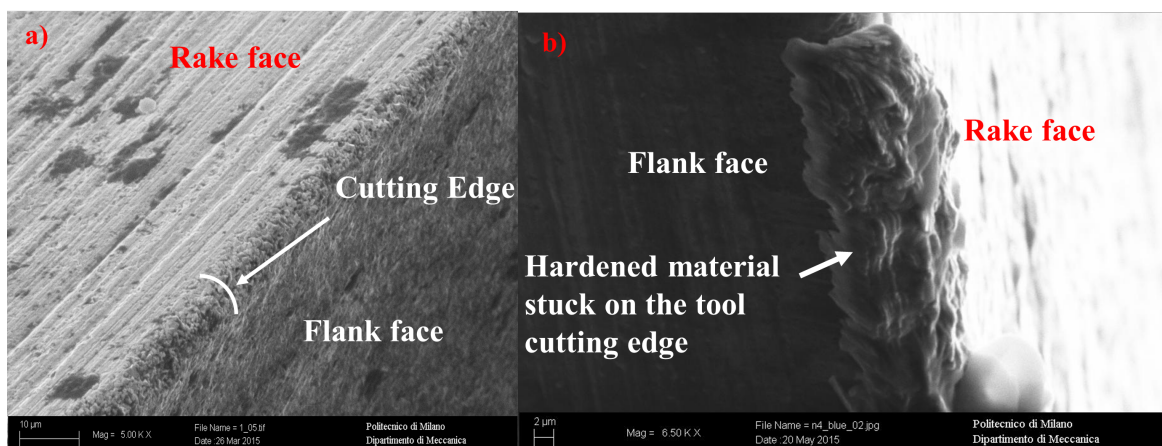

Figure 6. SEM images: a) fresh tool; b) material stuck on the tool cutting edge (r_e = 9 μm, t_u = 6 μm, v_c = 300 m/min)

3.3. Experimental responses

During each experiment, the cutting and thrust force components (respectively, the forces in X and Z directions) are acquired using a Kistler 9257BA triaxial piezoelectric load cell and the mean values of both force signals throughout the steady cutting phase are calculated. After each cutting test, the chips are collected for offline measuring their thickness by means of Alicona Infinite Focus, as depicted in Figure 7. Each chip is measured perpendicularly to its lateral surface in five different positions along its length and the chip thickness value t_c is calculated as the mean of these five measurements. Table 3 shows the experimental results for cutting force, thrust force and chip thickness.

Table 3. Experimental results

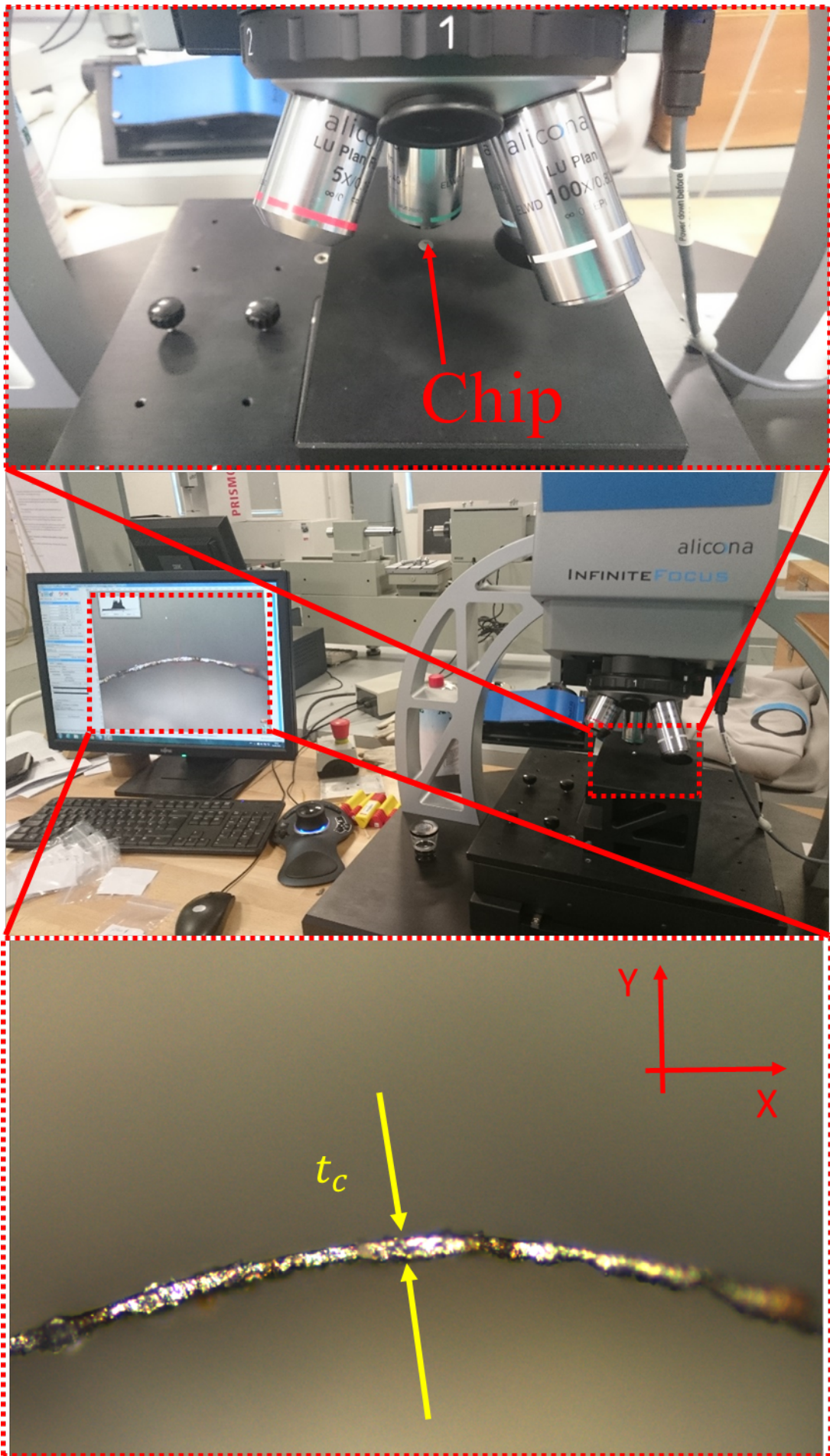| Experimental condition		Cutting force F_c (N)		Thrust force F_t (N)		Chip thickness t_c (µm)	
		Replicate 1	Replicate 2	Replicate 1	Replicate 2	Replicate 1	Replicate 2
a	v_c = 100 m/min t_u = 6 µm	13.15	12.68	5.88	5.38	13.92	14.15
b	v_c = 300 m/min t_u = 6 µm	10.91	11.15	5.66	6.15	12.32	17.40
c	v_c = 100 m/min t_u = 9 µm	16.67	16.74	6.20	7.00	17.64	17.20
d	v_c = 300 m/min t_u = 9 µm	15.15	15.04	8.07	8.27	15.73	16.79

Figure 7. Chip thickness (t_c) measurements

The percentage error between experimental process outputs and predicted results is calculated as follows:

$$err_i = \frac{|experimental\ value - predicted\ value|}{experimental\ value} \cdot 100 \quad\quad (5)$$

where the subscript i becomes "c", "t" and "tc" when the considered process output is, respectively, the cutting force, the thrust force or the chip thickness. These errors are calculated with respect to the mean value of experimental results that are reported in Table 3.

4. Results and discussion

The results obtained with developed finite element model implementing ALE approach and artificially introduced DMC are discussed in this section and compared with the results obtained with a rounded tool edge. FEM results are compared with experiments.

As shown in Figure 8a, when considering a rounded tool edge, an area exists beneath the edge where the material speed is extremely low. This zone is claimed to be DMC in some studies[19,20], but here neither the total speed (Figure 8a) nor its components along cutting and thrust direction are uniformly equal to 0 m/s and this fact is against the basic condition of DMC stationary nature. Figure 8d shows the velocity components v_1 and v_2 (respectively in cutting and thrust direction) for 5 nodes selected on the arbitrary line AB drawn below the tool edge radius. For example, v_1 and v_2 of node 5 are 0.0519 m/s and 0.0325 m/s respectively, thus violating the DMC stationary nature. On the other hand, Figure 8b proves that the introduction of DMC as a totally rigid body joint to the tool could allow a proper modeling of micromachining with DMC since the workpiece material is able to flow over a region of static material.

In Figure 8a and 8b, a shear plane is defined as the line OS connecting the stagnation point (S) to the pre-flow zone and parallel to the velocity contour plot boundary between the region with the maximum workpiece velocity (red region in Figure 8a) and the region with the material velocity after

entering primary deformation zone (yellow region in Figure 8a). Line OS is used as reference to extract representative values of quantities as the Von Mises stress, the equivalent plastic strain and temperature for further analyses (Section 4.1).
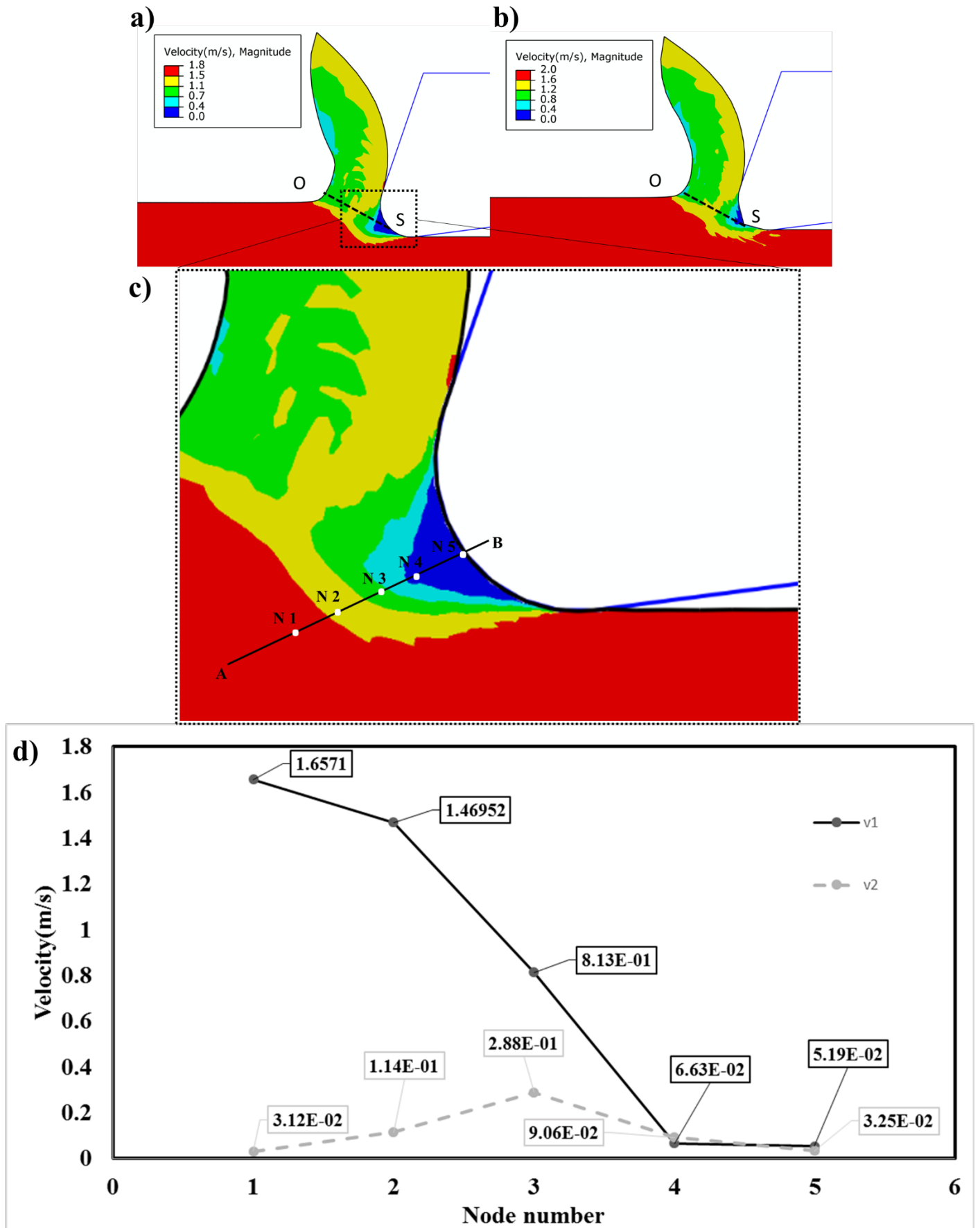
Figure 8. a) Velocity distribution for a rounded tool edge; b) velocity distribution for tool with DMC - Case 4 ($\psi = 15°, \zeta = 15°$); c) arbitrary line AB passing by DMC; c) velocity magnitude of v_1 and v_2 along line

AB for 5 nodes [all graphs are extracted after a simulation time = 0.045 ms and refer to the experimental condition with v_c = 100 m/min, and t_u = 9 μm]

4.1. Workpiece stress, strain and temperature

The maximum and minimum values of Von Mises stress, equivalent plastic strain and temperature along the shear plane OS (Figure 8a and 8b) have been extracted from FEM output and represented in Figure 9, 10 and 11, respectively. All graphs show that the analyzed quantities depend on DMC.
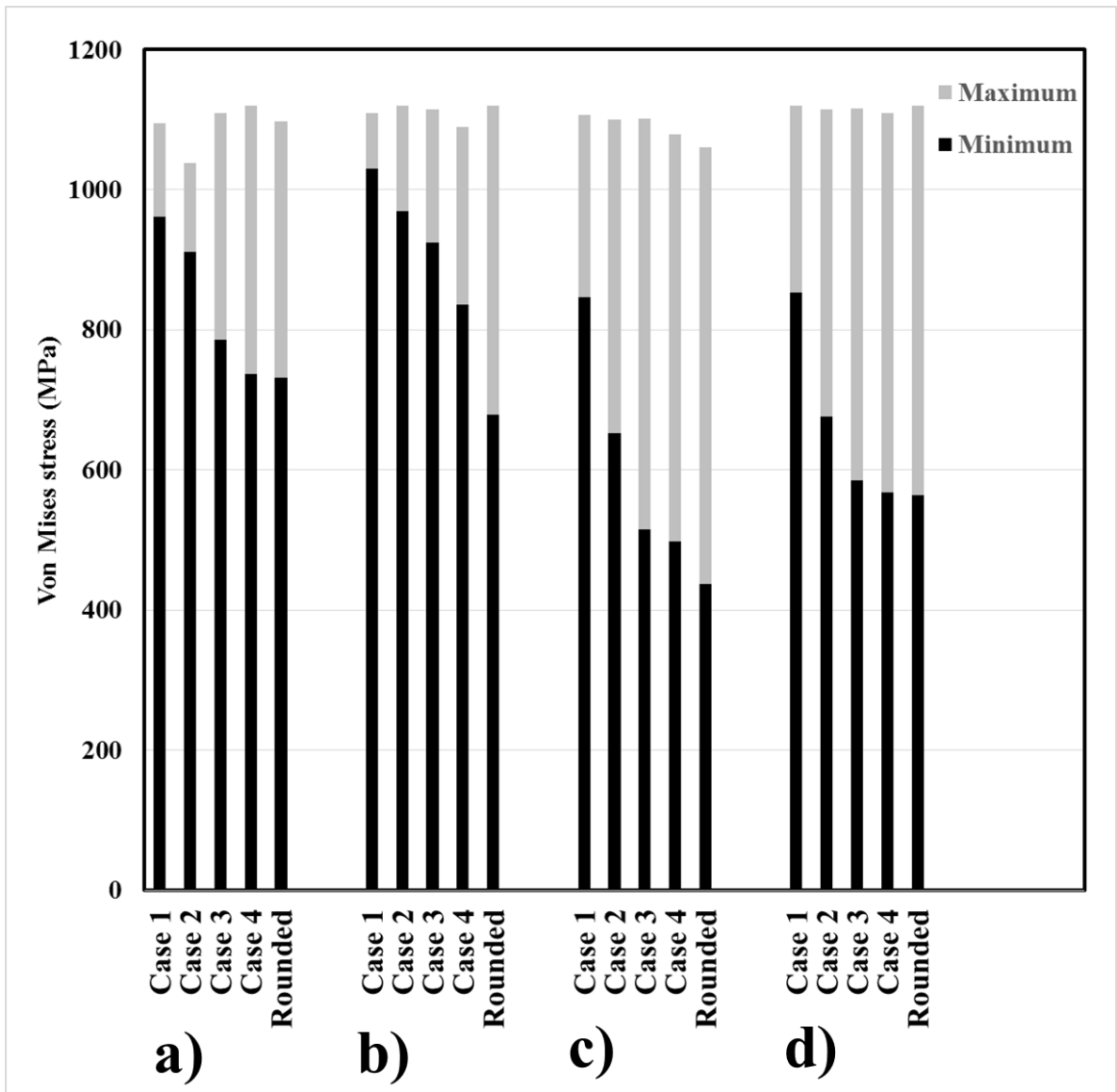
Figure 9. Maximum and minimum Von Mises stress on the shear plane OS in the experimental conditions with: a) v_c = 100 m/min, t_u = 6 μm; b) v_c = 300 m/min, t_u = 6 μm; c) v_c = 100 m/min, t_u = 9 μm; d) v_c = 300 m/min, t_u = 9 μm
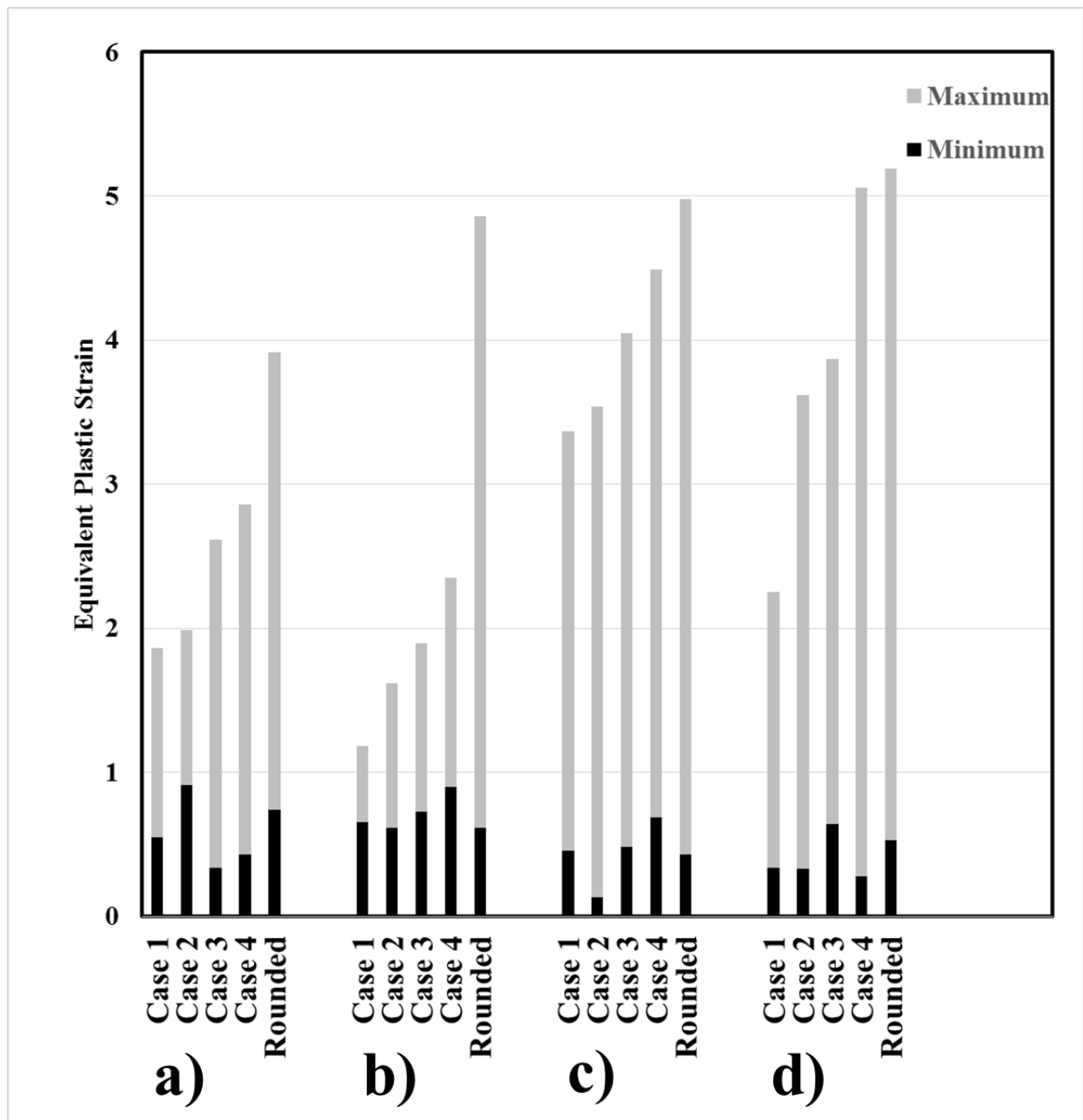
Figure 10. Maximum and minimum equivalent plastic strain on the shear plane OS in the experimental conditions with: a) v_c = 100 m/min, t_u = 6 μm; b) v_c = 300 m/min, t_u = 6 μm; c) v_c = 100 m/min, t_u = 9 μm; d) v_c = 300 m/min, t_u = 9 μm

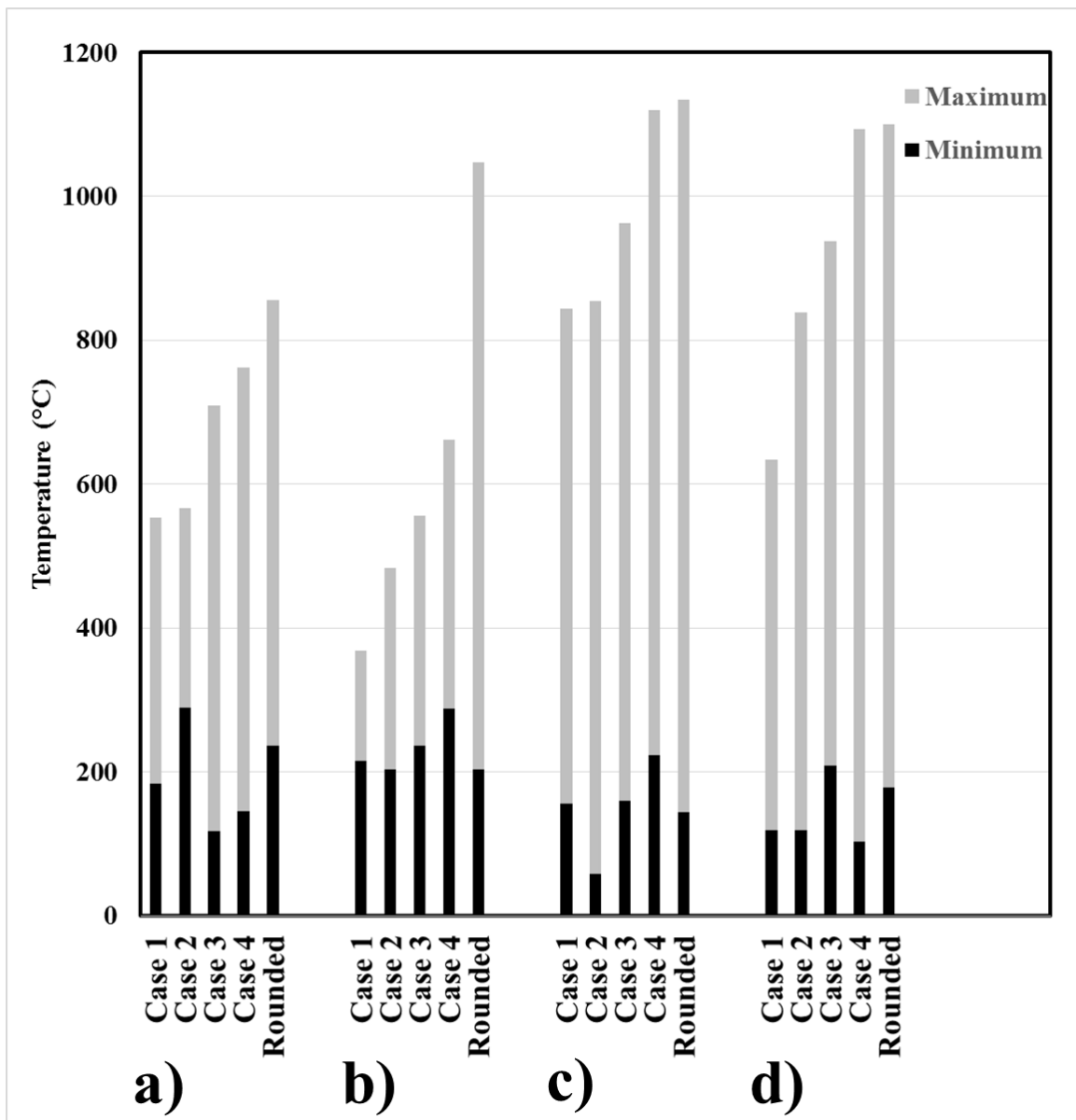*Figure 11. Maximum and minimum temperature on the shear plane OS in the experimental conditions with:*

a) v_c = 100 m/min, t_u = 6 μm; b) v_c = 300 m/min, t_u = 6 μm; c) v_c = 100 m/min, t_u = 9 μm;

d) v_c = 300 m/min, t_u = 9 μm

Figure 9 shows that the difference between maximum and minimum Von Mises stress (grey part of the graph) is higher for simulations with rounded tool edge than in case of models with DMC (the lowest difference occurs for the DMC geometry of Case 1 for experimental conditions b, c and d. DMC changes the nature of tertiary shear zone that is caused by the friction between tool rounded cutting edge and workpiece[18,39]. In fact, the DMC presence avoids the direct contact between tool edge and chip. In simulations with rounded edge tool

(Figure 8a), the shear plane OS passes through both primary and tertiary shear zones and this can be the reason for a high stress variation (Figure 9). On the other hand, in simulation with DMC (Figure 8b) the shear plane OS passes only through the primary shear zone, because the tertiary shear zone is located under the DMC clearance face and above the DMC rake face.

Figure 10 and Figure 11 respectively show the difference between maximum and minimum equivalent plastic strain and temperature along the shear plane OS. Both quantities assume the highest values for all machining conditions when simulations are performed considering a rounded tool edge, hence the DMC introduction decreases equivalent plastic strain and temperature on the shear plane. This fact means that the situation inside the chip is more homogeneous with the DMC introduction.

4.2. Chip formation

The chip formation provides a lot of valuable information about the metal cutting process. For example, the chip formation is of interest because the Chip Compression Ratio (CCR) is an indicator of total plastic deformation of the target material [40]. In micromachining, where tool edge radius plays a fundamental role, the chip formation analysis becomes very important also because of the MUCT phenomenon. DMC affects the tool-chip interaction and, thus, the final chip thickness by changing the cutting operation geometry. For this reason, the DMC effect on chip thickness has been investigated by comparing FEM and experimental results.

Figure 12 shows the errors between the measured and the predicted chip thickness (err_{tc}) in case of different DMC geometries and rounded tool edge. The experimental chip thickness measurement procedure is described in Section 3.3 while the chip thickness predicted by FEM has been calculated as the mean value of five measurements taken along the chip length at the simulation final stage. Data point out that DMC existence and geometry affect the chip thickness prediction performance. In particular, the DMC geometry of Case 2 provides the lowest prediction error in all cutting conditions except for experimental condition a) ($v_c = 100$ m/min, $t_u = 6$ μm), for which the FE simulation with rounded edge gives the lowest error for

cutting force and chip thickness. This fact implies that Case 2 is likely to represent the DMC geometry closest to the real one at least in some cutting conditions. However, further analysis on cutting forces (Section 4.3) are needed to confirm this result.
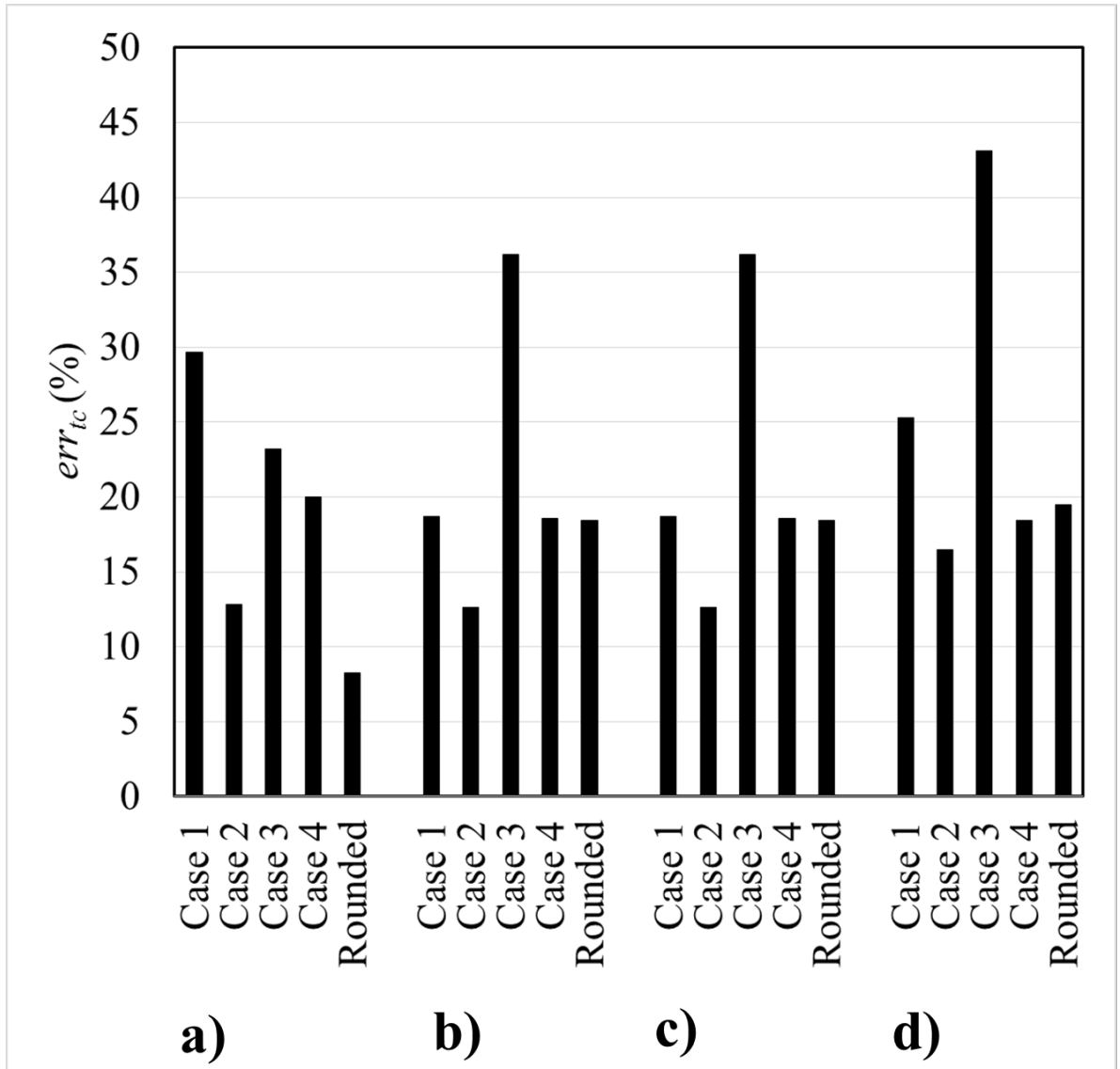

Figure 12. Percentage error for chip thickness prediction (err$_{tc}$) in the experimental conditions with: a) v_c = 100 m/min, t_u = 6 μm; b) v_c = 300 m/min, t_u = 6 μm; c) v_c = 100 m/min, t_u = 9 μm; d) v_c = 300 m/min, t_u = 9 μm

As an example, Figure 13 depicts the chip geometry and the Von Mises stress distribution for the different DMC geometries and rounded tool edge in the cutting condition c) (v_c = 100 m/min, t_u = 9 μm). The DMC rake face, which is associated to the angle ζ, is responsible for

pushing the chip away from the tool-workpiece interface. It can be observed that chip curl is more pronounced with $\zeta = 15°$ (Figure 13b and 13d) than with $\zeta = 0°$ (Figure 13a and 13c), that is when the tool rake angle becomes negative due to DMC rake angle. Kountanya and Endres[10] speculated that a greater chip curl is due to a lower shear angle and a higher strain in chip material, which are caused by a negative rake angle. FE model results are in accordance with this hypothesis.

The DMC clearance angle ψ changes the primary and tertiary shear zone location and pushes the region with higher stress away from the tool clearance face. As shown in Figure 13a and 13b, $\psi = 0°$ pushes the region with higher stress in front of the tool edge while in the other cases (Figure 13c, 13d and 13e) this region extends towards the tool clearance face. This observation leads to conclude that DMC can help to protect the tool clearance face from experiencing high stress and may help to prevent a tool severe wear.
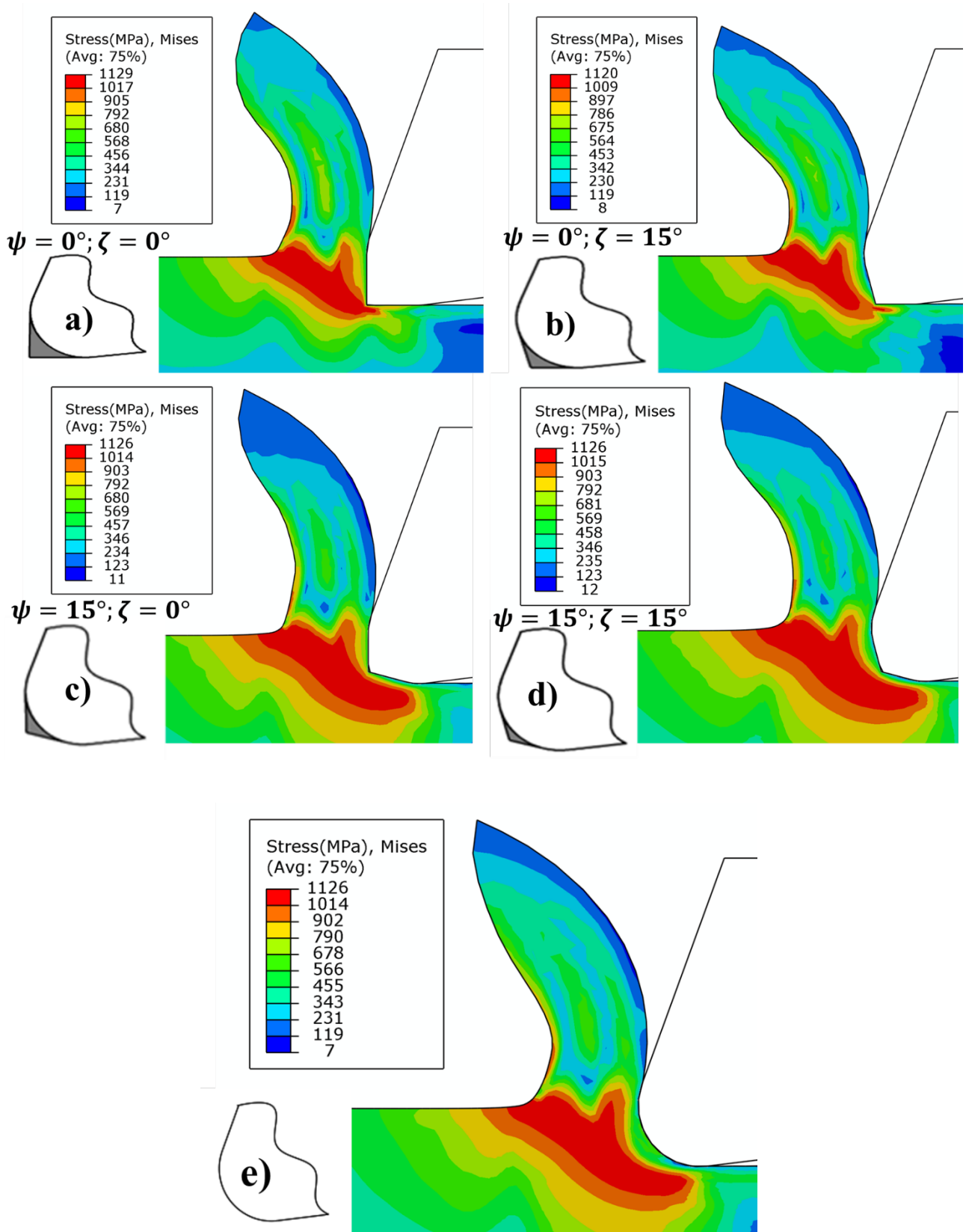
Figure 13. Stress distribution for different DMC geometries in the experimental conditions with

v_c = 100 m/min, t_u = 9 μm: a) Case 1 (ζ = 0°, ψ = 0°); b) Case 2 (ζ = 15°, ψ = 0°); c) Case 3 (ζ = 0°, ψ = 15°); d) Case 4 (ζ = 15°, ψ = 15°); e) rounded tool edge [all graphs are extracted after a simulation time = 0.045 ms]

4.3. Cutting forces

The errors between predicted and experimental results for the cutting force (Figure 14) and the thrust force (Figure 15) point out that the DMC geometry has a strong influence on the cutting force prediction. In particular, introducing the DMC geometry of Case 2 allows a prediction performance improvement for both force components, except for the experimental condition a) ($v_c = 100$ m/min, $t_u = 6$ μm) in case of cutting force (Figure 14). In addition, DMC introduction is more effective in case of thrust force, for which the lowest percentage error is 3.14% for the cutting condition b) with $t_u = 6$ μm and $v_c = 300$ m/min (Figure 15). These results could support the assumption that Case 2 represents better the real DMC geometry.
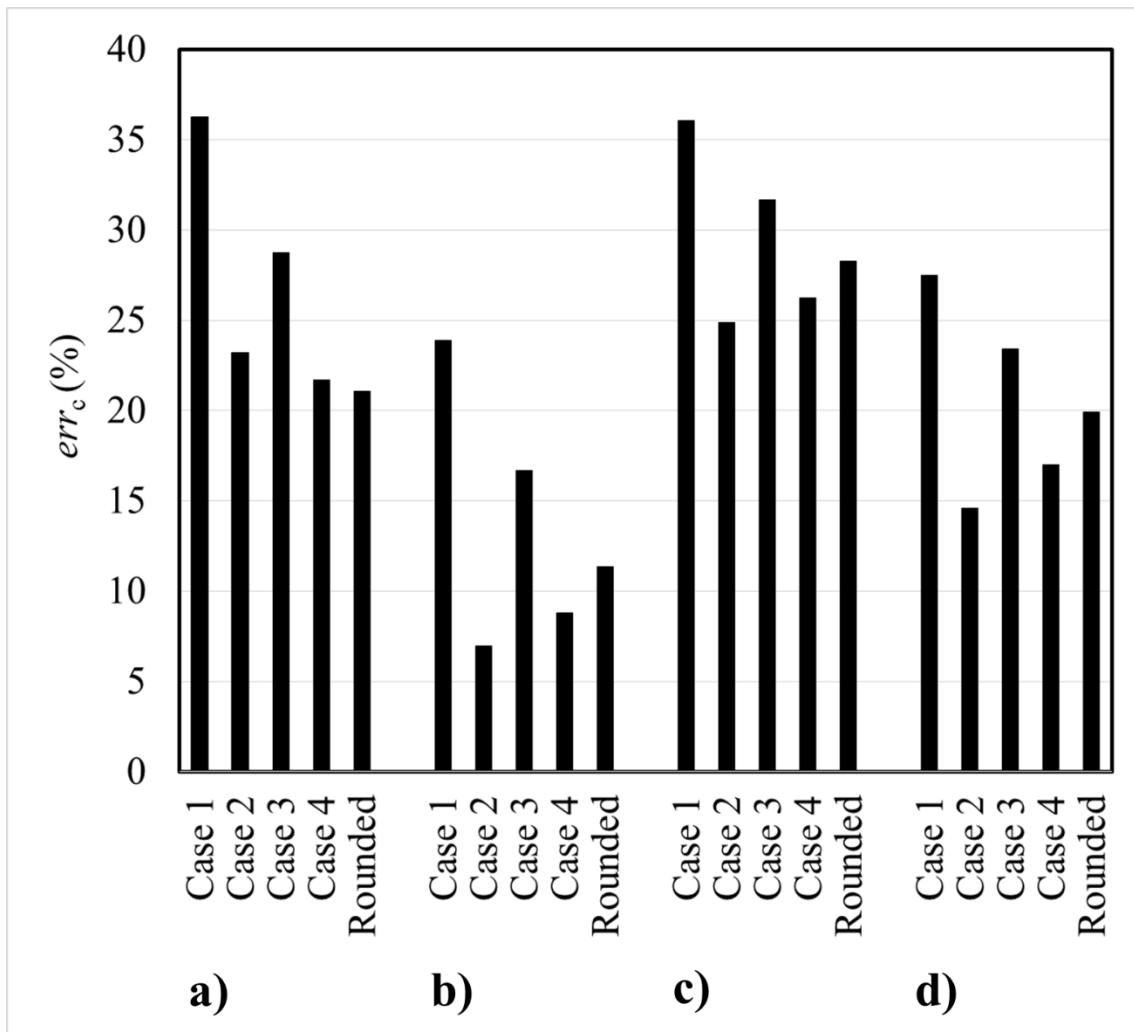

Figure 14. Percentage error for cutting force prediction (err$_c$) in the experimental conditions with: a) $v_c = 100$ m/min, $t_u = 6$ μm; b) $v_c = 300$ m/min, $t_u = 6$ μm; c) $v_c = 100$ m/min, $t_u = 9$ μm; d) $v_c = 300$ m/min, $t_u = 9$ μm
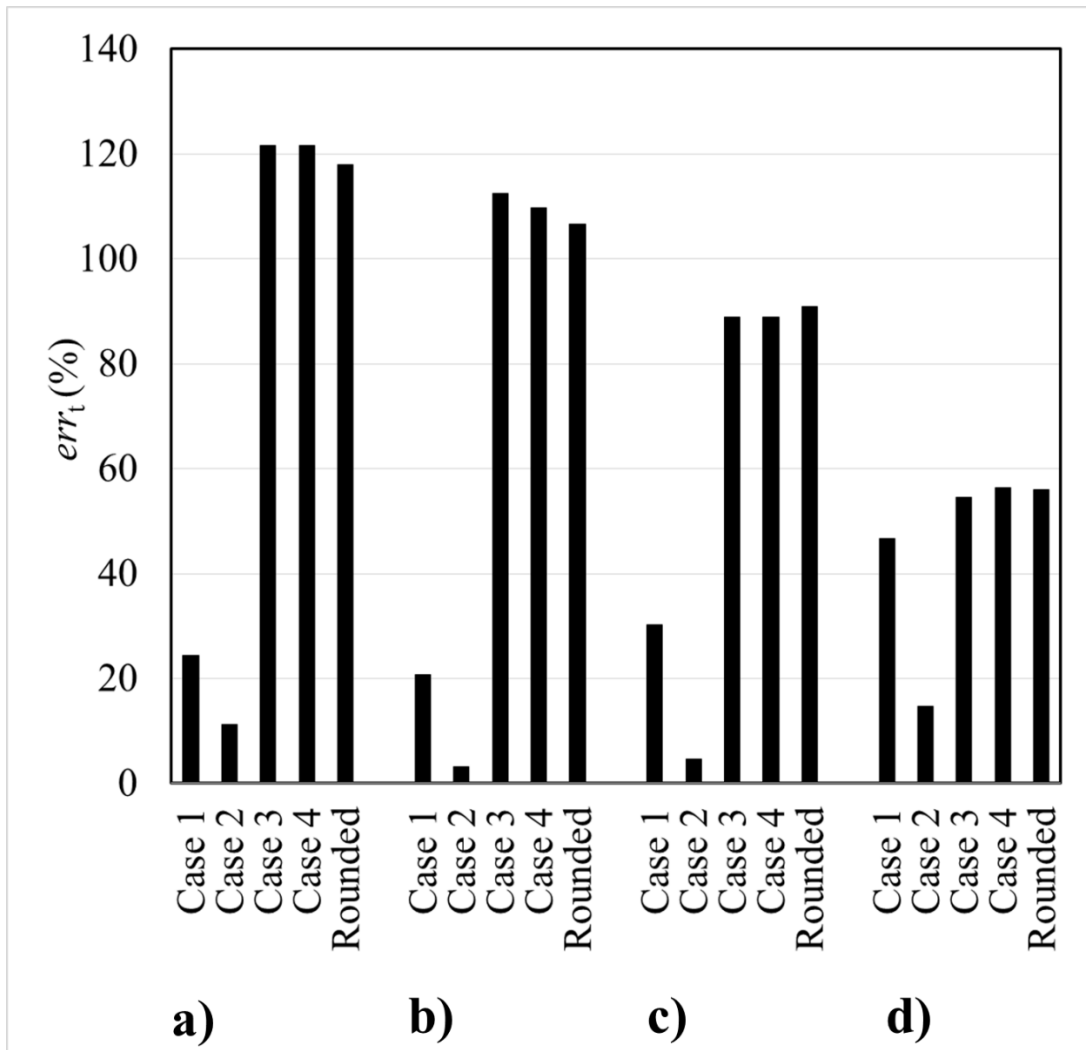
Figure 15. Percentage error for thrust force prediction (err$_t$) in the experimental conditions with: a) $v_c = 100$ m/min, $t_u = 6$ μm; b) $v_c = 300$ m/min, $t_u = 6$ μm; c) $v_c = 100$ m/min, $t_u = 9$ μm; d) $v_c = 300$ m/min, $t_u = 9$ μm

5. Conclusions and future developments

This study aims to model and simulate the micro orthogonal cutting in presence of DMC in order to investigate the effects of this phenomenon on the micromachining process outputs (cutting force, thrust force, chip thickness) and stress distribution, equivalent plastic strain and temperature inside the workpiece shear zones. Current FE model approaches based on state of the art assumptions cannot take into account the DMC stationary properties. For this purpose, a suitable FE model was

developed by artificially introducing the DMC on the rounded tool edge and four DMC geometries were tested.

Based on the performed analyses, the following concluding remarks can be drawn:

1. Finite element simulations show how the Von Mises stress, equivalent plastic strain and temperature distribution on the shear plane are dependent on DMC presence and geometry.

2. By comparing experimental data with FEM results, it is shown how errors associated to cutting force, thrust force and chip thickness are highly sensitive to the DMC presence and geometry. The prediction performance of FE models can be significantly improved by introducing the DMC. For instance, it is possible to reduce the error between simulated results and experiments to less than 5% in case of thrust force predictions.

3. The DMC geometry of Case 2 ($\zeta = 15°, \psi = 0°$) provides the lowest errors for cutting force, thrust force and chip thickness in all cutting conditions except for a), where simulation with a rounded tool edge provides the lowest errors for cutting force and chip thickness. Therefore, Case 2 is likely to represent the DMC geometry closest to the real one at least in some cutting conditions.

4. According to FEM results, the DMC geometry of Case 2 also introduces a more homogeneous distribution of the Von Mises stress, equivalent plastic strain and temperature along the shear plane.

This study demonstrates how the DMC introduction in Finite Element Modeling of micro orthogonal cutting process is able to improve the simulation performances. Nevertheless, future studies will aim at improving the model prediction performances by a more accurate modeling of the tool-DMC-chip contact and the target material constitutive behavior.

References

1. Takács M, Verö B, Mészáros I. Micromilling of metallic materials. *J Mater Process Technol* 2003; 138: 152–155.

2. Fang FZ, Venkatesh VC. Diamond Cutting of Silicon with Nanometric Finish. *CIRP Ann - Manuf Technol* 1998; 47: 45–49.

3. Liu FZF and YC. On minimum exit-burr in micro cutting. *J Micromechanics Microengineering* 2004;

14: 984.

4.   Mian A., Driver N, Mativenga PT. Identification of factors that dominate size effect in micro-machining. *Int J Mach Tools Manuf* 2011; 51: 383–394.

5.   Chae J, Park SS, Freiheit T. Investigation of micro-cutting operations. *Int J Mach Tools Manuf* 2006; 46: 313–332.

6.   Abdelmoneim ME, Scrutton RF. Tool Edge Roundness and Stable Build-Up Formation in Finish Machining. *J Manuf Sci Eng* 1974; 96: 1258–1267.

7.   Waldorf DJ, DeVor RE, Kapoor SG. A Slip-Line Field for Ploughing During Orthogonal Cutting. *J Manuf Sci Eng* 1998; 120: 693–699.

8.   Zhang HT, Liu PD, Hu RS. A three-zone model and solution of shear angle in orthogonal machining. *Wear* 1991; 143: 29–43.

9.   Warnecke G. New method of visualizing the cutting process. *1977 Manuf Eng Trans* 1977.

10.   R.K. Kountanya WJE. A high magnification experimental study of orthogonal cutting with edge-honed radius. In: *Proceedings of ASME International Mechanics Engineering Congress and Exposition*. New York, 2001.

11.   Jacobson S, Wallén P. A new classification system for dead zones in metal cutting. *Int J Mach Tools Manuf* 1988; 28: 529–538.

12.   Wallén P, Jacobson S, Hogmark S. Intermittent metal cutting at small cutting depths—1. Dead zone phenomena and surface finish. *Int J Mach Tools Manuf* 1988; 28: 515–528.

13.   Jacobson S, Wallén P, Hogmark S. Intermittent metal cutting at small cutting depths—2. Cutting forces. *Int J Mach Tools Manuf* 1988; 28: 551–567.

14.   Arrazola PJ, Özel T, Umbrello D, et al. Recent advances in modelling of metal machining processes. *CIRP Ann - Manuf Technol* 2013; 62: 695–718.

15.   Waldorf DJ, DeVor RE, Kapoor SG. An Evaluation of Ploughing Models for Orthogonal Machining. *J Manuf Sci Eng* 1999; 121: 550–558.

16.   Karpat Y, Özel T. Mechanics of high speed cutting with curvilinear edge tools. *Int J Mach Tools Manuf* 2008; 48: 195–208.

17.   Jun MB, Liu X, DeVor RE, et al. Investigation of the Dynamics of Microend Milling—Part I: Model Development. *J Manuf Sci Eng* 2006; 128: 893–900.

18.   Fang N. Slip-line modeling of machining with a rounded-edge tool—Part I: new model and theory. *J Mech Phys Solids* 2003; 51: 715–742.

19.   Movahhedy MR, Altintas Y, Gadala MS. Numerical Analysis of Metal Cutting With Chamfered and Blunt Tools. *J Manuf Sci Eng* 2002; 124: 178–188.

20.   Wan L, Wang D. Numerical analysis of the formation of the dead metal zone with different tools in orthogonal cutting. *Simul Model Pract Theory* 2015; 56: 1–15.

21.   Childs THC. Ductile shear failure damage modelling and predicting built-up edge in steel machining. *J Mater Process Technol* 2013; 213: 1954–1969.

22.   Weule H, Hüntrup V, Tritschler H. Micro-Cutting of Steel to Meet New Requirements in Miniaturization. *CIRP Ann - Manuf Technol* 2001; 50: 61–64.

23.   Systèmes D. Abaqus analysis user's manual. *Simulia Corp Provid RI, USA* 2007.

24.   Rakotomalala R, Joyot P, Touratier M. Arbitrary Lagrangian-Eulerian thermomechanical finite-element model of material cutting. *Commun Numer Methods Eng* 1993; 9: 975–987.

25.   Özel T, Zeren E. Finite element modeling the influence of edge roundness on the stress and temperature fields induced by high-speed machining. *Int J Adv Manuf Technol* 2007; 35: 255–267.

26.   Woon KS, Rahman M, Neo KS, et al. The effect of tool edge radius on the contact phenomenon of tool-based micromachining. *Int J Mach Tools Manuf* 2008; 48: 1395–1407.

27.   Jin X, Altintas Y. Prediction of micro-milling forces with finite element method. *J Mater Process Technol* 2012; 212: 542–552.

28.   Mabrouki T, Rigal J-F. A contribution to a qualitative understanding of thermo-mechanical effects during chip formation in hard turning. *J Mater Process Technol* 2006; 176: 214–221.

29.   Movahhedy M, Gadala MS, Altintas Y. Simulation of the orthogonal metal cutting process using an arbitrary Lagrangian–Eulerian finite-element method. *J Mater Process Technol* 2000; 103: 267–275.

30.   Pantalé O, Bacaria J-L, Dalverny O, et al. 2D and 3D numerical models of metal cutting with damage effects. *Comput Methods Appl Mech Eng* 2004; 193: 4383–4399.

31.   Movahhedy MR, Gadala MS, Altintas Y. SIMULATION OF CHIP FORMATION IN ORTHOGONAL METAL CUTTING PROCESS: AN ALE FINITE ELEMENT APPROACH. *Mach Sci Technol* 2000; 4: 15–42.

32.   Limido J, Espinosa C, Salaün M, et al. SPH method applied to high speed cutting modelling. *Int J Mech Sci* 2007; 49: 898–908.

33.   Ben Moussa N, Sidhom H, Braham C. Numerical and experimental analysis of residual stress and plastic strain distributions in machined stainless steel. *Int J Mech Sci* 2012; 64: 82–93.

34.   Outeiro JC, Umbrello D, M'Saoubi R, et al. Evaluation of Present Numerical Models for Predicting Metal Cutting Performance And Residual Stresses. *Mach Sci Technol* 2015; 19: 183–216.

35.   Arrazola PJ, Özel T. Investigations on the effects of friction modeling in finite element simulation of machining. *Int J Mech Sci* 2010; 52: 31–42.

36.   Johnson GR, Cook WH. A constitutive model and data for metals subjected to large strains, high strain rates and high temperatures. In: *Proceedings of the 7th International Symposium on Ballistics*. The Hague, The Netherlands, 1983, pp. 541–547.

37.   Jaspers SPF., Dautzenberg J. Material behaviour in conditions similar to metal cutting: flow stress in the primary shear zone. *J Mater Process Technol* 2002; 122: 322–330.

38.   Haglund AJ, Kishawy HA, Rogers RJ. An exploration of friction models for the chip–tool interface using an Arbitrary Lagrangian–Eulerian finite element model. *Wear* 2008; 265: 452–460.

39.   Jin X, Altintas Y. Slip-line field model of micro-cutting process with round tool edge effect. *J Mater Process Technol* 2011; 211: 339–355.

40.   Astakhov VP. *Tribology of metal cutting*. Elsevier, 2006.